Journal of
Materials Chemistry A

Accepted Manuscript

This is an *Accepted Manuscript*, which has been through the RSC Publishing peer review process and has been accepted for publication.

Accepted Manuscripts are published online shortly after acceptance, which is prior to technical editing, formatting and proof reading. This free service from RSC Publishing allows authors to make their results available to the community, in citable form, before publication of the edited article. This *Accepted Manuscript* will be replaced by the edited and formatted *Advance Article* as soon as this is available.

To cite this manuscript please use its permanent Digital Object Identifier (DOI®), which is identical for all formats of publication.

More information about *Accepted Manuscripts* can be found in the **Information for Authors**.

Please note that technical editing may introduce minor changes to the text and/or graphics contained in the manuscript submitted by the author(s) which may alter content, and that the standard **Terms & Conditions** and the **ethical guidelines** that apply to the journal are still applicable. In no event shall the RSC be held responsible for any errors or omissions in these *Accepted Manuscript* manuscripts or any consequences arising from the use of any information contained in them.

Oxalate route for promoting activity of manganese oxide catalysts in total VOCs oxidation: effect of calcination temperature and preparation method

Wenxiang Tang [a,c], Xiaofeng Wu[a], Dongyan Li[a,c], Zhen Wang[b], Gang Liu[a,c], Haidi Liu[a], Yunfa Chen*[a]

Received (in XXX, XXX) Xth XXXXXXXXX 20XX, Accepted Xth XXXXXXXXX 20XX
DOI: 10.1039/b000000x

A novel template-free oxalate route was applied to synthesize mesoporous manganese oxides with high surface area (355 $m^2 g^{-1}$) and well-defined mesopores which can be obtained in large quantities. The physicochemical properties of the materials were characterized by means of TG, XRD, SEM, TEM, H_2-TPR and XPS techniques. All catalysts were tested on catalytic deep oxidation of benzene, and the effects of calcination temperature on the features of catalyst structure and catalytic activity were investigated. Manganese oxides prepared by oxalate route exhibited better catalytic activities for complete oxidation of benzene, toluene and o-xylene as compared with related manganese oxides prepared by other different methods (NaOH route, NH_4HCO_3 route and nanocasting strategy), and especially the temperature for benzene conversion of 90% on the oxalate-derived manganese oxide catalysts was 209 °C which is 132°C lower than required for the catalyst prepared by NaOH route. The catalytic performance of manganese oxide is correlated with surface area, pore size, low-temperature reducibility and distribution of surface species. The mole ratio of Mn^{4+}/Mn^{2+} on the samples which performed better catalytic activity was close to 1.0 and it was good for the redox process of $Mn^{4+}\leftrightarrow Mn^{3+}\leftrightarrow Mn^{2+}$ which is the key factor in determining the activity on MnOx, further indicating that oxalate route is good for keeping the distribution of manganese oxidation state at a appropriate degree. A possible process of VOCs complete oxidation on manganese oxide catalysts is discussed. In addition, the best catalyst was highly stable with time on stream and resistant to water vapor.

[a] *Institute of Process Engineering, Chinese Academy of Sciences, Beijing, China 100190. E-mail: yfchen@mail.ipe.ac.cn; Fax: +86 10 8254 4896; Tel: +86 10 8254 4896*
[b] *CAS Key Laboratory of Standardization and Measurement for Nanotechnology, National Center for Nanoscience and Technology, Beijing, China 100190,*
c University of Chinese Academy of Sciences, Beijing, China 100049,

1. Introduction

Volatile organic compounds (VOCs) emitted from industrial process and fossil fuels' combustion can cause many environmental problems, such as ozone generation, photochemical smog and so on[1-3]. Low concentration of VOCs will also be a great threat to the human beings' health[4, 5] and the abatement of VOCs is highly desirable. Many methods (e.g. absorption, thermal combustion, biofiltration, catalytic oxidation) have been used to remove the hazardous VOCs in recent years[6-11].

Journal of Materials Chemistry A Accepted Manuscript

However, catalytic oxidation is a perfect way to reduce VOCs at low concentration and it can be operated at lower temperature (300-600°C) than thermal combustion which requires additional fuels and forms thermal NO_x[9, 12]. Compared to absorption method, catalytic oxidation can keep a good performance longer and have a great economic advantage[12]. Supported noble metal as Pt[13, 14], Pd[15, 16], Au[17, 18], Ag[19, 20] catalysts are known to be very active for deep oxidation of VOCs. Though precious metal catalysts exhibit high activity at very low temperature, they can't be used in industrial processes widely because of their high cost and some related problems, such as volatility, sintering and susceptibly poisoning tendency. Compared to noble metal, many active transition metal oxides (Fe_2O_3, Cr_2O_3, CuO, NiO, CeO_2, MnO_2 and Co_3O_4)[21-27] are cheaper and easier to be obtained as catalysts for combustion of VOCs.

Among the active oxide catalysts for VOCs combustion, manganese oxides such as Mn_3O_4, $Mn_2O_3$and MnO_2[20, 28-33]are known for exhibiting good activity in combustion of hydrocarbons and also considered as environmentally friendly materials. Gandhe et al.[34] showed that cryptomelane-type octahedral molecular sieve (OMS-2) catalyst had highly efficient activity for the total oxidation of ethyl acetate which was ascribed to the presence of Mn^{4+}/Mn^{3+} type redox couples and facile lattice oxygen on catalysts. Meanwhile, OMS-2 have also been found to be very active for VOCs oxidation in Santos et al.'s publication[31] and Mn_3O_4 could significantly improve the mobility and reactivity of lattice oxygen, but Mn_2O_3 has the opposite effect. Kim et al.[30] reported a series of manganese oxides catalysts (Mn_3O_4, Mn_2O_3 and MnO_2) for VOCs combustion and the promoted effect of other metals (K, Ca, Mg). They found the sequence of catalytic activity was Mn_3O_4 >Mn_2O_3 >MnO_2 which was highly correlated with the oxygen mobility and the surface area of the catalysts. It is notable to point out that the oxygen mobility can be enhanced by the oxygen vacancies existing on the catalysts[35] and the lattice oxygen donating abilities over manganese oxides also make a great contribution on the catalytic oxidation[36]. Moreover, the existence of higher manganese oxidation state (Mn^{4+}) in catalysts plays an important role in improving catalytic activity for VOCs combustion[37] which may be ascribed to the good ability of adsorbing oxygen. Pozan[38] have discussed the effect of support on catalytic activity of manganese oxide catalyst for toluene combustion and the manganese states and oxygen species play an important role in the catalytic activity. Therefore, the activity for VOCs combustion on manganese oxides is mainly determined by three factors: the surface area; the distribution of manganese state; the active oxygen species including adsorbed oxygen, oxygen vacancy and lattice oxygen.

Herein, we present work that significantly promotes the activity of manganese oxides for VOCs combustion by using a novel mesoporous structure catalyst with high surface area. The catalysts with high surface area are synthesized by an oxalate rout which can be obtained in large quantities. BTX (benzene, toluene and xylene), three major categories of VOCs, are mainly emitted from newly developed building materials, coating operations, motor fuels, and steel manufacturing industries and are most difficult to oxidize completely among environmental pollutants. In this study, we explore the catalytic properties of this kind of manganese oxides for BTX oxidation and compared it to other MnOx prepared by different methods. A strong correlation between manganese states and oxygen species is found on the catalysts and the possible mechanism of BTX deep oxidation over manganese oxides is discussed.

2. Experimental details

2.1 Catalyst synthesis

2.1.1 Oxalate route

An oxalate route was applied to the catalysts preparation. All chemicals used in this study including $Mn(NO_3)_2$ (50 wt.%) solution, $(NH_4)_2C_2O_4$ (99.9%) and absolute alcohol (99.9%) were all purchased from Xilong Cop. (china) without further purification. The water used to prepare all solutions was made from Millipore Milli-Q water (15MΩ cm). Typically, 48 mmol $(NH_4)_2C_2O_4$ was dissolved in 200 mL water to form a clear solution which was quickly added to the 200 mL manganese ion solution with a mole concentration of 0.2 M under strong stirring at room temperature (about 25 °C). The precipitation happened in several seconds. After stirring for 40 min, one precipitation (precursor A) was filtered directly and another (precursor B) was aged for further 24h under static condition in order to get two kinds of oxalate precursors with different structure. Both precipitants were filtered, washed with deionized water three times and absolute ethanol one time, then dried at 80 °C for 24 h. The oxide catalysts were obtained by sintering the precursors in a muffle furnace at a ramp of 2 °C min^{-1} from room temperature (RT) to a certain temperature and kept at this temperature for 5 h. The temperature of calcination varied from 350 °C to 550 °C and

Journal of Materials Chemistry A Accepted Manuscript

the products were denoted A-T (or B-T) (T represents the different calcination temperature included 350 °C, 450 °C and 550 °C).

2.1.2 Precipitation using NaOH or NH_4HCO_3

In a typical synthesis, 100 mL 0.48 M NH_4HCO_3 (or NaOH) solution was added to 100 mL 0.2 M $Mn(NO_3)_2$ solution under vigorously stirring and the mixed solution was aged for 4h at room temperature. The final white or brown precipitate was filtered and washed three times with water and ethanol, dried at 80 °C for 12 h. These two samples were heated at 450 °C for 5 h (heating rate 2 °C min^{-1}) in air and denoted as sample C-450 (NH_4HCO_3 route) and sample E-450 (NaOH route).

2.1.3 Nano-casting strategy

SBA-15 silica was used as a hard template for nanocasting and a simple "two-solvent" approach[39, 40] was introduced to synthesize another kind of mesoporous manganese oxide. Firstly, 2.5 g mesoporous SBA-15 was dispersed in 120 mL of dry n-hexane and further stirred at room temperature for 4 h. Then, a desired volume of $Mn(NO_3)_2$ (50 wt.%, Xilong) solution (quantity corresponding to the pore volume of SBA-15 template determined by N_2 sorption) was added slowly with strong stirring. After stirring vigorously for 12 h at room temperature the mixture was filtered and dried at 40 °C for 48 h. Afterwards, the sample was calcined at 450 °C for 5 h (heating rate 2 °C min^{-1}) in air. The resulting materials were treated three times with a 2 M NaOH solution, to remove the silica template, washed with water several times, and then dried at 80 °C. This procedure results in another mesoporous manganese oxide which is denoted as sample D-450.

2.2 Characterization of catalysts.

X-ray diffraction (XRD) patterns of the catalysts were measured on a Panalytical X'Pert PRO system using Cu-Kα radiation in the diffraction angle (2θ) range 5°–90°. Crystal phase were identified by using X'pert HighScore software to refer the related peaks to the standard powder diffraction in database (ICDD PDF2-2004). The specific surface areas and pore size distribution of all catalysts were obtained with N_2 adsorption-desorption method on an automatic surface analyser (AS-1-C TCD, Quantachrome Cor., USA). Before measurement, every sample was degassed at 200 ℃ for 3 h. The thermal gravimetric analysis (TGA) of precursors (A and B) was performed using an HCT-2 TGA/DTA system in air with a heating-rate of 10 °C min^{-1}. The morphology images of samples were recorded on a scanning electron microscopy (SEM, JEOL JSM-6700F, Japan, 15 kV, 10 μA). The microstructures of samples (A-450, C-450, D-450, and E-450) were obtained using transmission electron microscopy (TEM, JEOL JEM-2010F) with an accelerating voltage of 200 kV. Surface species of the as-prepared catalysts were determined by X-ray photoelectron spectroscopy (XPS) using an XLESCALAB 250Xi electron spectrometer from VG Scientific with a monochromatic Al Kα radiation. Hydrogen temperature programmed reduction (H_2-TPR) was carried out in a U-shaped quartz reactor under a gas flow (5% H_2 balanced with Ar, 25 mL min^{-1}). In each procedure, 30mg catalyst (40~60 mesh) was used and the temperature was raised to 750 °C from room temperature at a constant rate 10 °C min^{-1}.

2.3 Catalytic activity tests

Performance of catalysts was evaluated in a continues-flow fixed-bed quartz microreactor (i.d. 6 mm) at a space velocity (SV) of 60000 mL g^{-1} h^{-1}. Catalysts (100 mg, 40~60 mesh) were loaded in the quartz reactor with quartz wool packed at both ends of the catalysts bed. The continuous flow (100 mL min^{-1}) was composed of air and 1000 (or 200) ppm of gaseous benzene (toluene, or o-xylene). For consideration of water vapour's effect, an air flow (50 mL min^{-1}) was used for bubbling water before mixed with another air flow containing gaseous benzene and the mixed gas that composed a relative water vapour (1%) and benzene (500 ppm) was used for catalytic test. The concentration of benzene in the effluent gas was analysed by a gas chromatograph (Shimadzu GC-2014) equipped with a flame ionization detector (FID) and the concentration of CO_2 in the outlet gas was detected by another FID with a methanizer furnace for converting CO_2 to CH_4. The complete conversion of BTX such as benzene ($W_{benzene}$, %) was calculated as follows:

$$W_{benzene} = C_{CO_2,\,out} / (C_{benzene,\,in} \times 6) \times 100\%$$

Where $C_{CO_2,\,out}$ (ppm) and $C_{benzene,\,in}$ (ppm) are the concentrations of CO_2 in the outlet gas and benzene in the inlet gas, respectively.

3 Results and discussion

3.1 TG and XRD analysis

Journal of Materials Chemistry A Accepted Manuscript

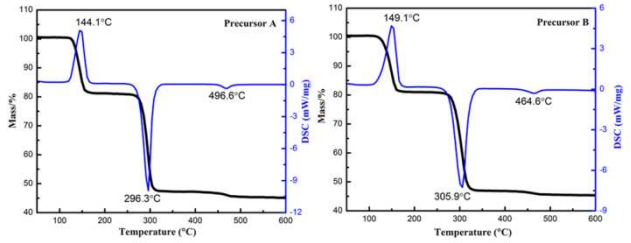

Fig. 1 Thermogravimetric (TG) analysis for the decomposition of manganese oxalate precursor A and B.

Fig. 1 shows the thermogravimetric analysis of two precursors. The first weight loss at 144.1 °C (A) or 149.1 °C (B) is corresponded to the dehydration of precursors to anhydrous manganese oxalate meanwhile the second weight loss is contributed to decomposition of manganese oxalate into manganese oxide. Both precursor A and B can be decomposed to manganese oxides at very low temperature and the converted temperature of sample B (305.9 °C) is a little higher than that of sample A (296.3 °C). The XRD patterns of precursors and as-calcined samples are shown in Fig. 2a-d. The two precursors obtained at different ageing time show different crystal phase as presented in Fig. 2a. The main diffractions of precursor A can be indexed to the $MnC_2O_4 \cdot 3H_2O$ (JCPDS PDF 032-0648) and a small part of $MnC_2O_4 \cdot 2H_2O$ (JCPDS PDF 025-0544). The peaks of precursor B reflect only the crystalline $MnC_2O_4 \cdot 2H_2O$ (JCPDS PDF 025-0544) which confirms that the precipitation is all converted to $MnC_2O_4 \cdot 2H_2O$ with increasing the ageing time. The calcination temperatures of precursors are arranged from 350 °C to 550 °C and the diffraction patterns of calcined catalysts are displayed in Fig. 2b and c. For the low calcination temperature (350 °C), no obvious peaks are obtained from their XRD patterns (A-350, B-350) which demonstrates they are amorphous or have poor crystallinity. When the calcination temperature is increased to 450 °C or 550 °C, the diffraction peaks are clearly appeared which are corresponded to the cubic crystal Mn_2O_3 (JCPDS PDF 001-1061). Interestingly, some obvious patterns are found in the catalysts A-450 as shown in Fig. 2b which confirms the occurrence of crystalline Mn_3O_4 (JCPDS PDF 001-1127) and this Mn_3O_4 crystalline are disappeared with developing the calcination temperature to 550 °C. Fig.2d shows the other manganese oxides synthesized by different methods and the diffraction patterns of sample C (NH_4HCO_3 route) and D (nanocasting route) can be indexed to MnO_2 (JCPDS PDF 001-0799). A pure phase of Mn_3O_4 (JCPDS PDF 001-1127) is observed on the catalyst E which is prepared by NaOH precipitation approach.

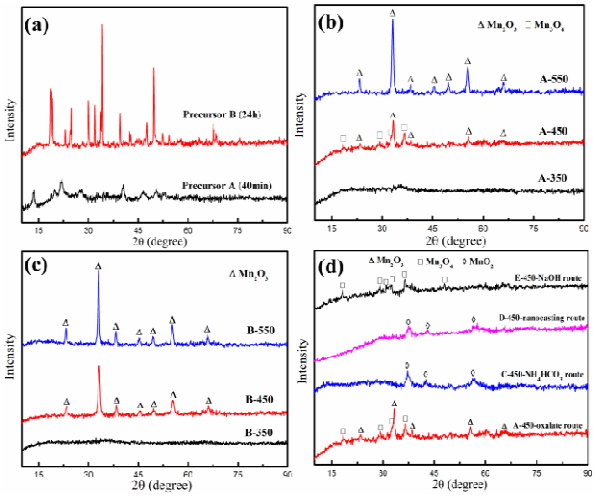

Fig. 2 XRD patterns of as-prepared precursors (a) and manganese oxides prepared by different methods (b, c, d).

3.2 Surface area and morphology

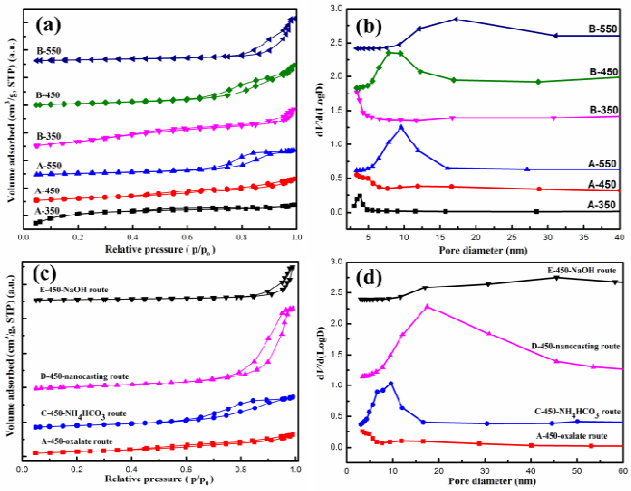

Fig. 3 N_2 adsorption-desorption isotherms curves (a,c) and pore size distribution calculated from desorption branch (b,d) of as-synthesized MnOx catalysts by oxalate route and other different methods.

Fig. 3 displays the N_2 adsorption-desorption isotherms and the pore size distribution of the catalysts A-T, B-T and other manganese oxides prepared by different methods. Obviously, a classical type IV isotherm is obtained and all the isotherms have a typical hysteresis loop which is often associated with narrow slit-like (micro-) pores and mesopores structure of the samples. From the data represented in Table 1, the catalysts treated at lower temperature (A-350, B-350) have larger surface area of 355.5 and 226.3 $m^2 \cdot g^{-1}$ while the samples calcined at higher temperature have a smaller surface area of 85.9 (A-450), 50.1 (A-550), 65.4

Journal of Materials Chemistry A Accepted Manuscript

(B-450), 35.1 (B-550) $m^2 \cdot g^{-1}$, respectively. However, the average pore size increases obviously with developing treatment temperature of catalysts. It is noticeable that the pore size distributions become wider when the calcination temperature is increased, indicating the irregular pore shapes is strongly affected by the treatment condition. Lower sintering temperature is good for keeping the original structure of precursor partly so that the samples have poor crystallinity and small pores. Meanwhile higher calcination temperature is favourable to achieve well crystallized particles and the growth of nanoparticle takes place gradually which will drive pore expansion and surface reduction. Therefore, the samples calcined at lower temperature is better for keeping small pores which will own more excellent catalytic properties because of the nano-effect of particles. Compared with the samples treated at 350 °C, the pore volume of A-450 or A-550 has a clear reduction (0.21→0.15 $cm^3 \cdot g^{-1}$) while just a small change is observed on the samples B-450 and B-550 (0.27 →0.25 $cm^3 \cdot g^{-1}$). As shown in Table1, the manganese oxides prepared by NH_4HCO_3 route and nanocasting approach both have a large surface area about 115.9 and 132.6$m^2 g^{-1}$ which are even lower than the samples prepared by oxalate route. However, the average pores of these samples are larger than A-450 obviously. Moreover, the pore volume of sample D-450-nanocasting-route has the highest value of 0.59 $cm^3 \cdot g^{-1}$ which may be ascribed to the ordered mesopores casted from SBA-15.

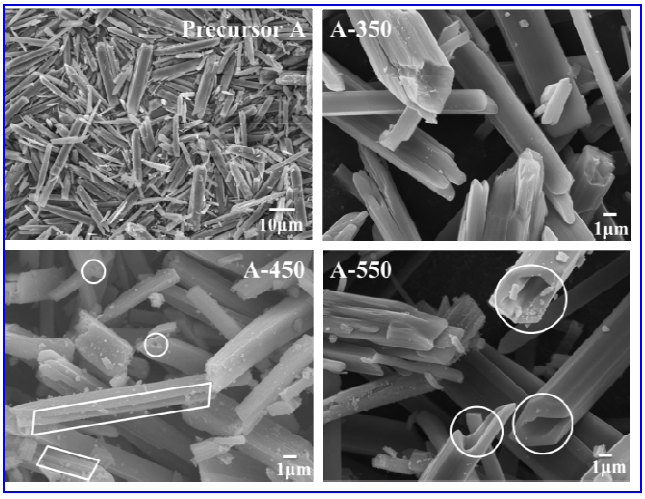

Fig. 6 SEM images of precursor A and related samples cancined at different temperature (350, 450 and 550 °C).

The SEM images of the precursors and related manganese oxide samples are shown in Fig. 6 and 7. It is observed that the precursors prepared from just 40 min stirring and another 24 h ageing were micro rods and butterfly-like plates. The diameter and length of the rods in the rod-like sample A are 2-4 μm and 30-50 μm, meanwhile the plates in sample B has 30 μm long and 20 μm wide but many plates have been broken down to smaller pieces. However, the micro rod of precursor A was kept very well after thermal treatment as shown in Fig. 4. Interestingly, the hollow structure (as presented in circle zone in Fig. 6) appeared in sample A-450 with a diameter of several hundred nanometres and it grew up to several micrometres in sample A-550 which is mainly caused by the expansion of pores. As shown in Fig. 7, the microstructure of sample B was decomposed to many fine particles after calcination process.

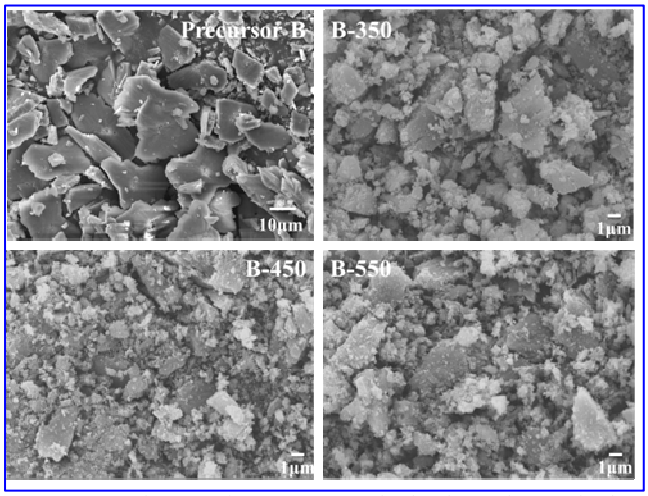

Fig. 7 SEM images of precursor B and related samples cancined at different temperature (350 °C, 450 °C, 550 °C).

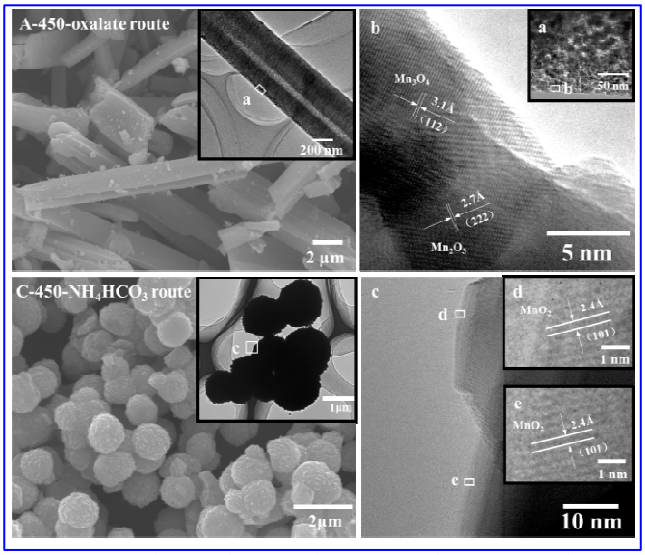

Fig. 8 SEM and TEM images of A-450 (oxalate route) and C-450 (NH_4HCO_3 route).

Fig.8 and 9 represent the microstructures of different manganese oxides with SEM and TEM images. It can be seen that there were mesoporous hollow rods with a diameter 1.5μm in sample A-450.

Journal of Materials Chemistry A Accepted Manuscript

From the high-resolution TEM (HRTEM) image of sample A-450, the intraplanar spacing are measured to be 0.31 nm and 0.27 nm which are in good consistence with that of the (112) and (222) crystal plane of the standard Mn_3O_4 (JCPDS PDF 001-1127) and Mn_2O_3 (JCPDS PDF 001-1061). The sphere-like manganese oxide prepared by NH_4HCO_3 precipitation method (C-450) is shown in Fig. 8 and its uniform diameter is about 1.5 μm. The clear intraplanar spacing from HRTEM is about 0.24 nm which is in agreement with (101) crystal phase of MnO_2 (JCPDS PDF 001-0799). With nanocasting process, manganese oxide ultrafine particles (<10nm) can be formed in the limited space of silicate pores and assembled to bundles of well-defined nanowires after removing hard template. Two typical intraplanar spacing about 0.31 and 0.24 nm can be obtained from HRTEM image which are assigned to (110) and (101) crystal phase of MnO_2 (JCPDS PDF 001-0799). The cube-like particle is observed in E-450 (NaOH route) and the main intraplanar spacing about 0.49 nm can be ascribed to (101) crystal plane of the standard Mn_3O_4 (JCPDS PDF 001-1127).

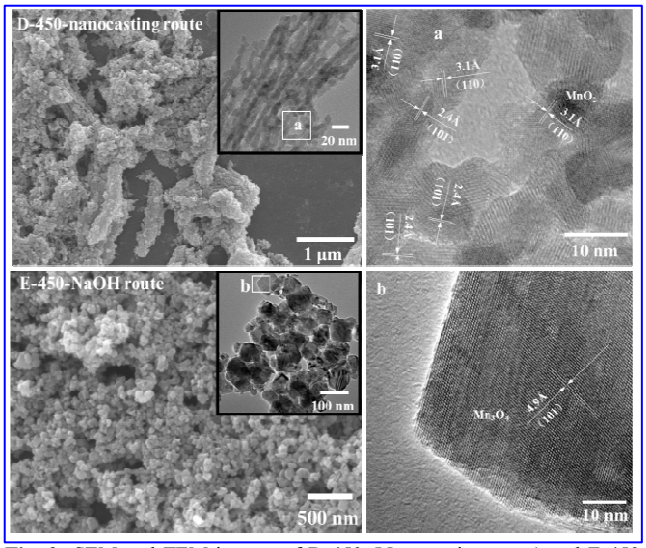

Fig. 9 SEM and TEM images of D-450 (Nanocasting route) and E-450 (NaOH route).

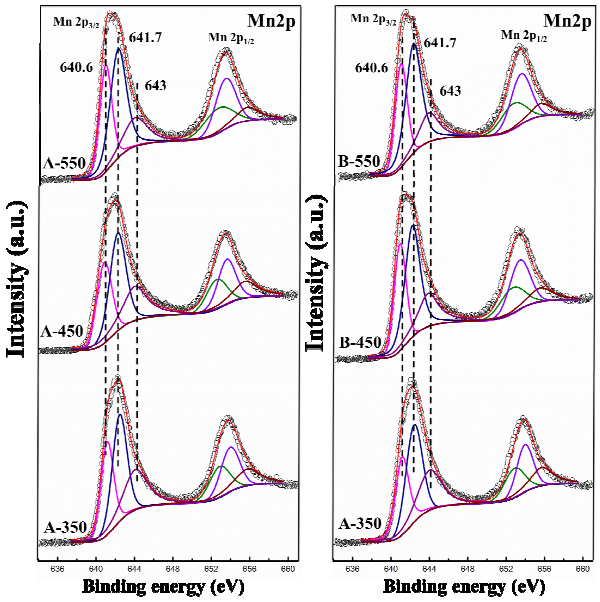

Fig. 10 Mn2p XPS spectra of MnOx catalysts (oxalate route).

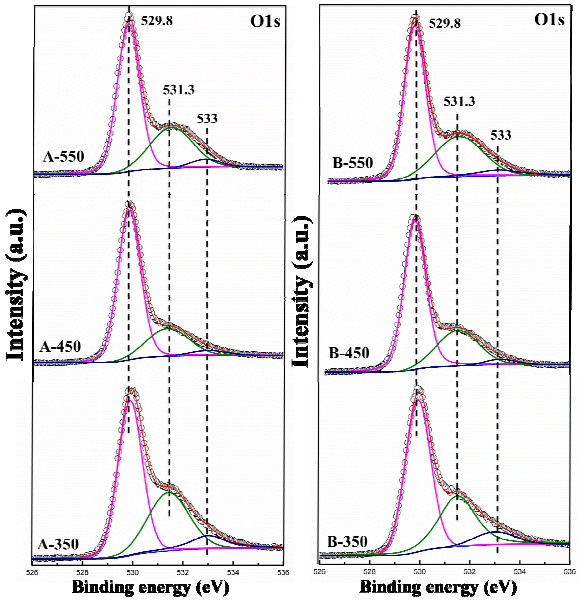

Fig. 11 O1s XPS spectra of MnOx catalysts (oxalate route).

3.3 Surface composition and oxidation state

The surface element compositions such as manganese oxidation states and adsorbed oxygen species were investigated by XPS method. Fig. 10 and 11 represent the Mn 2p and O 1s XPS spectras of the manganese oxide samples, respectively. As revealed in Fig. 10, the Mn 2p spectra of all samples are decomposed into three components corresponding to Mn(II), Mn(III) and Mn(IV) species on the surface of catalysts and an energy separation of 11.4~11.6 eV is observed between the Mn 2p3/2 and Mn 2p1/2 states. Fig 10 shows that the components at

Journal of Materials Chemistry A Accepted Manuscript

binding energies(BE) = 640.6±0.2, 641.7±0.2, and 643±0.2 eV are assigned to the surface Mn^{2+}, Mn^{3+}, and Mn^{4+} species, [28, 31, 41-44] respectively. The accurate content of surface Mn^{n+} and their molar ratios was calculated by a quantitative analysis method on the Mn2p XPS spectra, as shown in Table 1. Obviously, the calcination temperature of catalysts has a great impact on the distribution of surface manganese ions. The population of higher Mn^{4+} species decreased apparently with increasing the calcination temperature, such as A-350 (0.304)→A-550 (0.208) and B-350 (0.307)→B-550 (0.192), which illustrates that the amorphous MnO_x formed at low calcination temperature is good for keeping higher metal ions on oxides' surface. In the meantime, the lower mole ratios of Mn^{4+}/ Mn^{2+} or Mn^{4+}/ Mn^{3+} appeared with higher calcination temperature. However, a large quantity of Mn^{2+} species are hold on the catalysts during thermal treatment because of the reducing atmosphere formed in the decomposition process of oxalate ligands which has been discussed in other report[45]. Interestingly, the number of Mn^{4+} and Mn^{2+} ions are very close on catalyst A-350, B-350 and A-450 which exhibited better catalytic activities (as shown in section 3.5). The relation among Mn^{2+}, Mn^{3+}, and Mn^{4+} on the surface of manganese oxides has an important impact on the surface oxygen species of oxides. For amorphous MnO_x, more higher manganese state (Mn^{4+}) will produce more surface adsorbed oxygen species, such as O_2^- ,O^- , and lower manganese state (Mn^{2+}) existed in the crystal will produce oxygen vacancy (V_o) which will promote the mobility of lattice oxygen. Meanwhile, the highly crystallinity of samples formed under higher treatment temperature will have a great content of lattice oxygen (O^{2-}) and all surface oxygen species will make a certain degree of contribution on the combustion of VOCs. These different effects are proved by investigating the result of O 1s XPS. As represented in Fig. 11, the asymmetrical O 1s signal can be fitted with three components: one peak at low BE (about 529.8 ev) which is assigened to the lattice oxygen (O^{2-}); another peak at the medium with a binding energy (531.3 eV) that is ascribed to the surface adsorbed oxygen (O_2^-, O^-, O_2^{2-}) ; the small peak at highest BE (533.0 eV) which is contributed to the adsorbed OH groups and molecular water[31, 46, 47]. The contents of different surface oxygen species with a binding energy at 529.8 and 531.3 eV were summarized in Table 1. As expected, the amorphous MOx(A-350, B-350) has more adsorbed oxygen species(O_2^-, O^-, O_2^{2-}) and the samples with high crystallinity oppositely have larger population of surface lattice oxygen species. It is found that the samples possessing rich adsorbed surface oxygen (A-350, B-350) or surface lattice oxygen (A-450) have a better catalytic activity for benzene oxidation (shown in section 3.5).

Fig. 12 shows the O 1s and Mn 2p XPS spectra of the manganese oxides catalysts obtained by different methods and the distribution of surface species is concluded in Table 1. For MnO_2 prepared by NH_4HCO_3 precipitation and nanocasting route, there is a small population of Mn^{2+} on the catalyst surface and the main manganese species is Mn^{4+} and Mn^{3+}. Meanwhile, more Mn^{2+} is obtained on the Mn_3O_4 catalyst (NaOH precipitation) and the proportion of Mn^{4+} decreased seriously. Compared to the sample A-450, the content of lattice oxygen species reduced obviously on other three kinds of manganese oxides prepared by different methods. Moreover, the ratio of Mn^{4+}/Mn^{2+} is far away from 1.0 and their catalytic activities were inferior to the manganese oxide prepared by oxalate route.

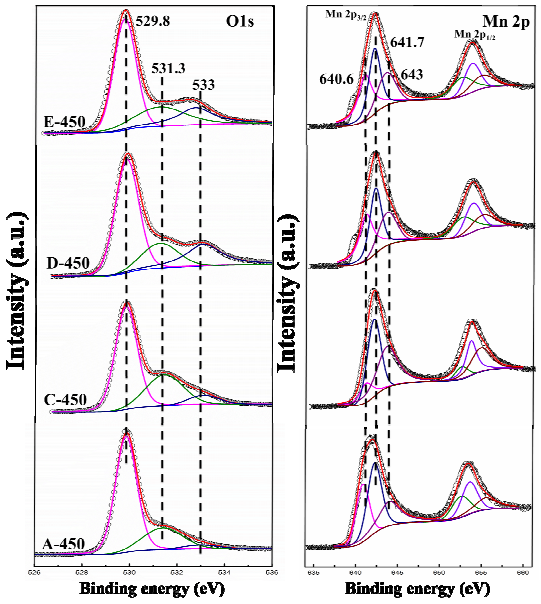

Fig. 12 O1s and Mn2pXPS spectra of MnOx catalysts prepared by different methods.

Table 1 Surface areas, average pore size, and pore volume from BET analysis and surface element compositions of the MnO_x samples from the Mn 2p and O 1 s XPS spectra.

sample	BET surface area ($m^2 \cdot g$)	BJH pore size (nm)	Pore volume ($cm^3 \cdot g^{-1}$)	surface element molar ratio						
				Mn					O	
				Mn^{2+}	Mn^{3+}	Mn^{4+}	Mn^{4+}/Mn^{2+}	Mn^{4+}/Mn^{3+}	Oads[a]	Olatt

Journal of Materials Chemistry A Accepted Manuscript

A-350	355.5	3.8	0.21	**0.301**	0.395	**0.304**	**1.010**	0.770	0.349	0.557
B-350	226.3	3.4	0.27	**0.300**	0.393	**0.307**	**1.023**	0.781	0.334	0.591
A-450	85.9	4.4	0.15	**0.290**	0.418	**0.291**	**1.003**	0.697	0.235	0.728
A-550	50.1	9.6	0.15	**0.325**	0.467	**0.208**	**0.641**	0.446	0.315	0.643
B-450	65.4	7.85	0.25	**0.297**	0.469	**0.234**	**0.787**	0.498	0.281	0.688
B-550	35.1	17.2	0.25	**0.306**	0.502	**0.192**	**0.626**	0.383	0.298	0.621
C-450	115.9	6.6	0.24	**0.126**	0.418	**0.456**	**3.624**	1.089	0.299	0.629
D-450	132.6	17.5	0.59	**0.144**	0.382	**0.473**	**3.284**	1.239	0.188	0.582
E-450	28.5	17.0	0.23	**0.391**	0.367	**0.242**	**0.619**	0.662	0.251	0.549

[a] adsorbed oxygen including O_2^-, O^- and O_2^{2-}

3.4 Temperature-programmed reduction

H_2-Temperature-programmed reduction analysis was operated to investigate the reducibility of Mn species or the reactivity of the oxygen species on the catalysts. According to the earlier publishing[31], the reduction of manganese oxides can be described by the successive processes: $MnO_2 \rightarrow Mn_2O_3 \rightarrow Mn_3O_4 \rightarrow MnO$. Every further reduction process will need a higher reaction temperature which gives us an effective method to determine the accurate composition of the catalysts. Fig. 13 displays the H_2-TPR profiles of the manganese oxide samples. Each profile was decomposed into two or three components which strongly depend on the oxidation states of the catalysts. All the TPR profiles show two separate peaks at higher temperature zone of which first reduction peak (250~320 °C) is corresponded to the reduction of Mn_2O_3 to Mn_3O_4 and second reduction peak (400~430 °C) is ascribed to the reduction of Mn_3O_4 to MnO. This result is in perfect agreement with the H_2-TPR results of manganese oxides reported in other literatures[30, 48]. It is worth to pointing out that the reduction temperatures of the samples treated at developing temperature shifts to higher value and it means the decrease of lattice oxygen mobility on catalysts. The oxygen mobility of catalysts will be an important factor on catalytic oxidation of VOCs[30, 49]. The clear peaks appeared at lower temperature zone (<250 °C) on catalysts A-350(or A-450, B-350) can be contributed to the reduction of higher metal ions (such as Mn^{4+}) to Mn_2O_3. However, the same peaks seem to diminish even disappear on the other samples which confirms the population of active Mn^{4+} is cut down by developing the calcination temperature of as-prepared catalysts. This result is consistent with the XPS data shown in Table1. Similarly, the perfect reducibility of the catalysts at lower temperature zone is up to the rich active oxygen species located on the catalysts surface which will have a great effect on the catalytic oxidation of VOCs. Therefore, we deduce that the catalysts (A-350, B-350, and A-450) with good reducibility at lower temperature will have a good performance on the deep oxidation of benzene. The reducibility properties of MnOx obtained by different methods are shown in Fig. 13c and the sample A-450 has the best reducibility at lower temperature zone compared with the other three kinds of manganese oxides.

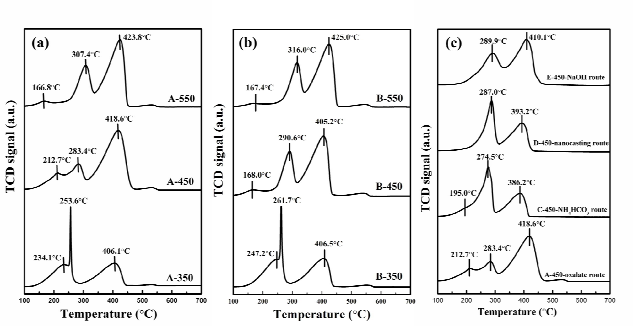

Fig.13 TPR profiles of MnOx catalysts.

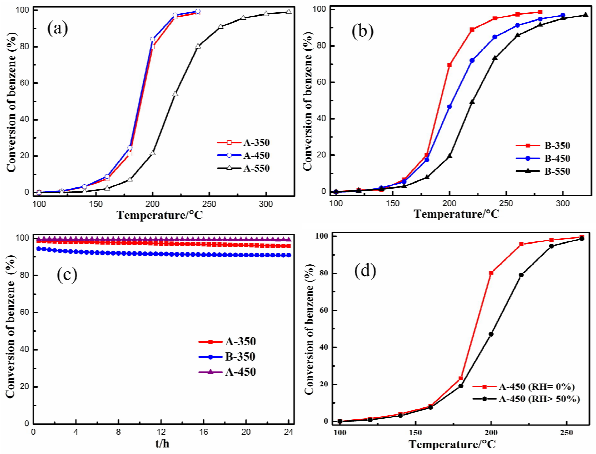

Fig. 14 (a, b) Benzene conversion as a function of reaction temperature over MnO_x catalysts under the conditions of benzene concentration =1000 ppm in air, SV= 60,000 mL g^{-1} h^{-1}; (c) Benzene oxidation over catalysts A-350, B-350, A-450 for 24 h on stream at 240 °C; (d) The effect of water vapor in feed stream on the benzene conversion over catalyst A-450 (benzene concentration is about 500 ppm in air, water vapor concentration > 1.56 %, SV= 60,000 mL g^{-1} h^{-1}).

3.5 Catalytic deep oxidation of VOCs

All oxalate-derived manganese oxide catalysts were investigated for the complete oxidation of benzene in the temperature range of

Journal of Materials Chemistry A Accepted Manuscript

100-350 °C, as represented in Fig. 14. The conversion of benzene to CO_2 increased with the rise in reaction temperature while CO_2 and H_2O were found to be the only products and the CO_2 selectivity was more than 99.0%, indicating that benzene can be completely oxidized over these catalysts. As shown in Fig. 14a and b, all catalysts show high activity towards the oxidation of benzene which is completely converted to CO_2 and H_2O at temperatures lower than 300 °C. In order to compare the catalytic activities of the samples conveniently, the temperature of conversion 10% ($T_{10\%}$), 50% ($T_{50\%}$), and 90% ($T_{90\%}$) are summarized in Table 2. It is concluded that the catalytic activity decreased in the order of A-350 ≈ A-450 ≈ B-350>B-450>A-550>B-550 and the catalysts treated at lower temperature perform better activities. The perfect activity on the amorphous catalysts (A-350 and B-350) can be contributed to the high surface area (A-350: 355.5 $m^2 g^{-1}$, B-350: 226.3 $m^2 g^{-1}$) and the rich surface adsorbed oxygen species and the good reducibility at the low temperature zone. For the highly crystalnility samples formed at higher temperature, the catalytic activity at lower temperature zone (<200 °C) decreased seriously except the catalyst A-450. The poor reducibility of the catalysts A-550, B-450, B-550 at lower temperature and the decreased value of surface area (as summarized in Table1) may be responsible for this phenomenon. Interestingly, the sample A-450 exhibited a best performance for benzene deep oxidation especially at 200 °C which may be associated to the good reducibility and the rich active lattice oxygen existed on this catalyst. The activities of some Mn-based catalysts reported in other literatures for benzene (or toluene) oxidation at 200 ℃ are listed in Table 3. As we can see, the catalysts in other reports have poor activity for benzene (or toluene) at 200 °C and the reaction rate for benzene oxidation at this temperature on our materials is about 2.25 mmol $g_{cat}^{-1} h^{-1}$ which is greater than others clearly. The evolutions with time-on-stream of benzene conversion at 240 °C for the catalysts including A-550, B-450, B-550 were shown in Fig. 14c. The catalytic activities of the catalysts were measured within 24 h and only a slight deactivation was observed on sample A-350 and B-350 which may be attributed to the amorphous crystal structures of the catalysts calcined at lower temperature (350 °C) are unstable under the reaction condition. However, the activity of A-350 is better than that of B-450 after 24 running which may be ascribed to that the sample A-350 has higher surface area and the mesoporous rod structure is more active and stable for benzene oxidation. Meanwhile, the result showed that the catalyst A-450 exhibited excellent catalytic activity and there was no significant drop in catalytic activity within 24 h running (99.5 % → 99.2 %), further indicating that this unsupported manganese oxide catalyst performs a perfect stability of catalytic activity and is equal even higher to many noble metal supported catalysts for benzene combustion in other reports[15-17, 50]. Furthermore, the effect of water vapor on the catalytic activity of A-450 was displayed in Fig.14d. It can be seen that the presence of water vapor had a negative effect on the catalyst. It suggested that many active sites were covered by the water vapor which competed with benzene molecules or oxygen molecules and it would lead to a reduction in the number of active sites which are available for the reaction of benzene[37, 51]. However, the complete oxidation of benzene under humid condition can be viewed at 250 °C and this activity is still better than many catalysts[21-23, 30].

The effect of preparation method on MnOx for catalytic oxidation of BTX (benzene, toluene, and xylene) was examined and the results are shown in Fig. 15. Generally, all the catalysts tested reveal high activity towards the oxidation of BTX. In terms of benzene oxidation, it is observed that the manganese oxides obtained by oxalate route performed much better than other samples even the surface area of A-450 is little smaller than C-450 and E-450. As expected, the catalytic activity decreased in the order of A-450-oxalate-route > C-450-$NH4HCO_3$-route > D-450-nanocasting-route > E-450-NaOH-route, coinciding with the sequences of surface lattice oxygen species concentration and low temperature reducibility. As shown in Table 2, the $T_{10\%}$, $T_{50\%}$, and $T_{90\%}$ values of A-450 (oxalate route) were ca. 164, 188, and 209 °C, which were 67, 102, and 132 °C lower than those achieved over the E-450-NaOH-route sample, respectively. Furthermore, the performances of catalysts for toluene and o-xylene oxidation are presented in Fig. 15b-c and the corresponding results are also displayed in Table 4. In terms of conversion into CO_2, the following performance trend was observed: A-450 > C-450 ≈ D-450 > E-450. In this case, the differences among the catalysts are less evident: both toluene and o-xylene are completely oxidized to CO_2 at 230-260 °C which may be ascribed to the low VOCs concentration tested in our research. However, the oxalate-derived manganese oxide exhibits better activity than the others especially at lower reaction temperature range (160-220 °C) due to the rich surface lattice oxygen species, mesoporous structure, low temperature reducibility and modest distribution of different

Journal of Materials Chemistry A Accepted Manuscript

manganese oxidation states.

Table 2. Catalytic activities of the as-prepared MnOx samples

catalyst	Preparation method	Benzene conversion (℃)			toluene conversion (℃)			o-xylene conversion (℃)		
		$T_{10\%}$	$T_{50\%}$	$T_{90\%}$	$T_{10\%}$	$T_{50\%}$	$T_{90\%}$	$T_{10\%}$	$T_{50\%}$	$T_{90\%}$
A-350	Oxalate route	164	190	212	-	-	-	-	-	-
A-450	Oxalate route	161	188	209	183	215	235	188	215	235
A-550	Oxalate route	185	218	258	-	-	-	-	-	-
B-350	Oxalate route	165	192	225	-	-	-	-	-	-
B-450	Oxalate route	168	203	258	-	-	-	-	-	-
B-550	Oxalate route	184	222	284	-	-	-	-	-	-
C-450	NH4HCO3 route	176	211	245	196	225	240	204	227	240
D-450	Nanocasting route	196	247	292	200	227	247	204	227	240
E -450	NaOH route	228	290	341	208	234	258	218	230	250

5

Table 3. Main data of research papers on VOCs (benzene or toluene) over manganese related oxides catalysts

Catalysts	Surface area ($m^2\ g^{-1}$)	VOC type	VOC conc. (ppm)	SV ($mL\ g_{cat}^{-1}\ h^{-1}$)	Conversion of VOC at 200 °C	Reaction Rate at 200 °C ($mmol\ g_{cat}^{-1}\ h^{-1}$)	Ref. no.
mesoporous MnO_2	266	toluene	1000	20,000	60%	0.54	52
MnO_2, Mn_2O_3	44~162	toluene	1000	20,000	40%	0.36	28
OMS	75.8	Benzene	627	48,000	45%	0.60	33
Cryptomelane (KMn_8O_{16})	45~84	Toluene	1062	16,000	< 5%	< 0.04	31
Mn_3O_4, Mn_2O_3, MnO_2	3~18	Benzene, toluene	1000	15,000	< 10%	< 0.07	30
LaMnO3.10	15~29	toluene	1000	20,000	<20%	< 0.18	53
$LaMnO_3$, $LaCoO_3$, $LaFeO_3$	4.8~17.2	Benzene	1000	60,000	< 10%	< 0.27	22
$CuO/Ce_{1x}MnxO_2$	7.2~158.4	Benzene	1000	12,000	70%	0.38	21
Pd/AlCe-PILC	343.6~377.4	Benzene	160	25,000	50%	0.09	15
$Pt/Mn/CeO_2$	60~100	Benzene	1000	20,000	75%	0.67	14
Manganese oxide	86~355	Benzene	1000		84.1%	2.25	
		toluene	1020	60,000	23.3%	0.64	This work
		o-xylene	230		20.4%	0.13	

Journal of Materials Chemistry A Accepted Manuscript

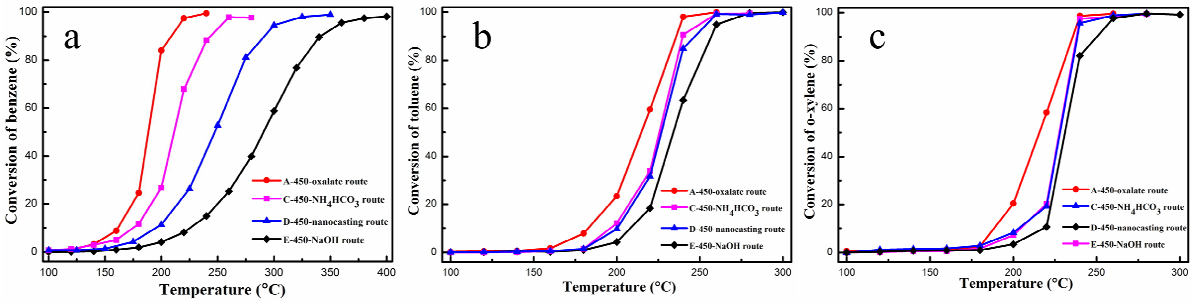

Fig. 15 BTX (a: benzene, 1000 ppm in air; b: toluene, 1020 ppm in air; o-xylene, 230 ppm in air) complete conversion as a function of reaction temperature over MnO_x catalysts synthesized by different methods. (SV= 60, 000 mL g^{-1})

3.6 Mechanism of VOCs oxidation over manganese oxide catalyst

It is noticeable that the distribution of surface species has a great impact on catalytic performance. It is well known that the catalytic activity on the manganese oxides is determined by several factors, such as lattice oxygen[30, 31], oxygen vacancy[28], adsorbed oxygen[21], surface area[36, 52], manganese oxidation state[36, 37] and so on. The possible processes of BTX such as benzene oxidation on the manganese oxide catalysts are discussed in Scheme 1. A strong relationship among these factors can be found. For an example, the population of adsorbed oxygen can be promoted by developing the content of manganese oxidation state (Mn^{4+}) on catalysts and the lower state (Mn^{2+}) will lead to generation of oxygen vacancy which is based on the principle of electro-neutrality. As shown in Scheme 1, the oxidation of VOCs by path 1and 2 is associated with adsorbed oxygen and oxygen vacancy which both have higher activity at lower temperature and enhance the adsorption and oxidation of benzene. However, the mole ratio of Mn^{2+}, Mn^{4+} and lattice oxygen on catalyst A-450 were all developed by the Mn_3O_4 phase existed in the Mn_2O_3 catalyst and this catalyst exhibited a highest activity in this research. In other words, the distribution of manganese states has a great impact on the catalytic performance and Mn_3O_4 can also promote the activity obviously. From the XPS data summarised in Table 1, it can be found that the mole ratios of Mn^{4+}/Mn^{2+}on the catalysts have better activity (A-350, B-350, A-450) are all close to 1.0. Therefore, this ratio of Mn^{4+}/Mn^{2+} on the manganese oxides is good for the redox process of $Mn^{4+}\leftrightarrow Mn^{3+}\leftrightarrow Mn^{2+}$ and this process is the key of benzene oxidation process on the catalysts. Xu et al.[54] demonstrated that the oxidation of CO on Mn_2O_3 might proceed through the Langmuir–Hinshelwood mechanism (<200 °C) to the Mars–van Krevelen mechanism(>350 °C) with increasing reaction temperature. In other words, the concentration of adsorbed hydrocarbon on the catalysts surface will increase quickly at elevated temperatures and more lattice oxygen will take part in the process of oxidation which can explain the sharp increasing of activity at higher reaction temperature (around 200 °C). Therefore, we assume that the hydrocarbon adsorbed on the higher manganese state site would be activated and the lattice oxygen will take part in the oxidation process (3rd pathway in Scheme 1). This will be an available explanation for the highest activity over the catalysts A-450 with highest ratio of lattice oxygen on the surface. All factors occurred on the manganese oxide catalysts in this study give rise to the high activity of VOCs combustion (4th general pathway in Scheme 1).

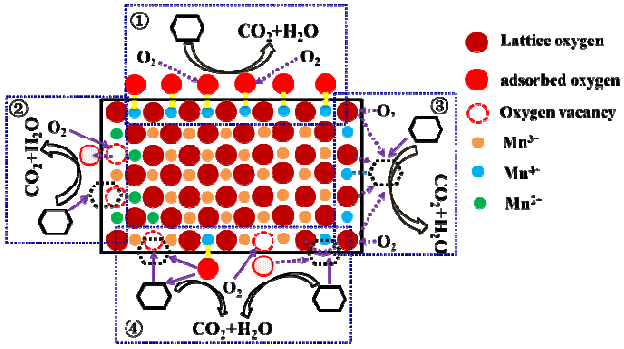

Scheme 1 The possible pathways for benzene oxidation on the MnOx catalyst

4. Conclusion

A series of mesoporous manganese oxides such as micro-rod, micro-tube and particles with high surface area and well-defined mesoporosities were successfully prepared by an oxalate route and examined for the gas-phase oxidation of benzene. The catalysts treated at lower temperature showed much better activity than the others for the catalytic oxidation of benzene, achieving 90% conversion to CO_2 below 220 °C. The characterization results showed that lower temperature of

Journal of Materials Chemistry A Accepted Manuscript

calcination was better for keeping high surface area and small pores while higher temperature treatment decreased the surface area and pore size. Moreover, the content of higher manganese oxidation state and adsorbed oxygen species were reduced obviously while lattice oxygen species were increased with developing the thermal treatment temperature which were also the key factors in determining the activity of MnO_x. Compared with other MnO_x obtained by different methods, oxalate-derived MnO_x exhibited higher activity for complete oxidation of BTX especially for benzene oxidation which was ascribed to their novel characteristics, such as large BET surface areas, small pores, low-temperature reducibility, rich lattice oxygen and appropriate distribution of manganese oxidation states. Moreover, these catalysts with mesoporous structure can be obtained in large quantities which will be a good candidate for VOCs abatement.

ACKNOWLEDGMENTS

This research was supported by the 863 Hi-tech Research and Development Program of China (Grant No. 2012AA062702), the Strategic Project of Science and Technology of Chinese Academy of Sciences (No. XDB05050000) and the National Natural Science Foundation of China (NSFC) (No. 51272253; No. 51002154).

Notes and references

1. R. Atkinson, *Atmospheric Environment*, 2000, **34**, 2063-2101.
2. A. P. Altshuller, *Atmospheric Environment (1967)*, 1983, **17**, 2131-2165.
3. W. P. L. Carter, *Atmospheric Environment. Part A. General Topics*, 1990, **24**, 481-518.
4. J. A. Bernstein, N. Alexis, H. Bacchus, I. L. Bernstein, P. Fritz, E. Horner, N. Li, S. Mason, A. Nel, J. Oullette, K. Reijula, T. Reponen, J. Seltzer, A. Smith and S. M. Tarlo, *The Journal of allergy and clinical immunology*, 2008, **121**, 585-591.
5. J. E. Cometto-Muñiz, W. S. Cain and M. H. Abraham, *Indoor Air*, 2004, **14**, 108-117.
6. G. Leson and A. M. Winer, *Journal of the Air & Waste Management Association*, 1991, **41**, 1045-1054.
7. K. Everaert and J. Baeyens, *Journal of hazardous materials*, 2004, **109**, 113-139.
8. K. L. Foster, R. G. Fuerman, J. Economy, S. M. Larson and M. J. Rood, *Chemistry of Materials*, 1992, **4**, 1068-1073.
9. J. J. Spivey, *Industrial & Engineering Chemistry Research*, 1987, **26**, 2165-2180.
10. T. D. Nguyen-Phan, M. B. Song and E. W. Shin, *Journal of hazardous materials*, 2009, **167**, 75-81.
11. M. Takeuchi, M. Hidaka and M. Anpo, *Journal of hazardous materials*, 2012, **237-238**, 133-139.
12. J. N. Armor, *Applied Catalysis B: Environmental*, 1992, **1**, 221-256.
13. X. Qian, D. Xiong, A. M. Asiri, S. B. Khan, M. M. Rahman, H. Xu and D. Zhao, *Journal of Materials Chemistry A*, 2013, **1**, 7525.
14. F. Liu, S. Zuo, X. Xia, J. Sun, Y. Zou, L. Wang, C. Li and C. Qi, *Journal of Materials Chemistry A*, 2013, **1**, 4089.
15. S. Zuo, Q. Huang and R. Zhou, *Catalysis Today*, 2008, **139**, 88-93.
16. J. M. Padilla, G. Del Angel and J. Navarrete, *Catalysis Today*, 2008, **133-135**, 541-547.
17. D. Andreeva, R. Nedyalkova, L. Ilieva and M. V. Abrashev, *Applied Catalysis B: Environmental*, 2004, **52**, 157-165.
18. C. Y. Ma, Z. Mu, J. J. Li, Y. G. Jin, J. Cheng, G. Q. Lu, Z. P. Hao and S. Z. Qiao, *Journal of the American Chemical Society*, 2010, **132**, 2608-2613.
19. M. A. Hernández, J. A. Velasco, M. Asomoza, S. Solís, F. Rojas and V. H. Lara, *Industrial & Engineering Chemistry Research*, 2004, **43**, 1779-1787.
20. Q. Ye, J. Zhao, F. Huo, J. Wang, S. Cheng, T. Kang and H. Dai, *Catalysis Today*, 2011, **175**, 603-609.
21. T.-Y. Li, S.-J. Chiang, B.-J. Liaw and Y.-Z. Chen, *Applied Catalysis B: Environmental*, 2011, **103**, 143-148.
22. H. Einaga, S. Hyodo and Y. Teraoka, *Topics in Catalysis*, 2010, **53**, 629-634.
23. Z. Mu, J. J. Li, M. H. Duan, Z. P. Hao and S. Z. Qiao, *Catalysis Communications*, 2008, **9**, 1874-1877.
24. A. Z. Abdullah, M. Z. Bakar and S. Bhatia, *Industrial & Engineering Chemistry Research*, 2003, **42**, 5737-5744.
25. J. S. Yang, W. Y. Jung, G. D. Lee, S. S. Park, E. D. Jeong, H. G. Kim and S.-S. Hong, *Journal of Industrial and Engineering Chemistry*, 2008, **14**, 779-784.
26. Y. Xia, H. Dai, H. Jiang, J. Deng, H. He and C. T. Au, *Environmental science & technology*, 2009, **43**, 8355-8360.
27. P. M. Kouotou, Z.-Y. Tian, H. Vieker, A. Beyer, A. Gölzhäuser and K. Kohse-Höinghaus, *Journal of Materials Chemistry A*, 2013, **1**, 10495.
28. F. Wang, H. Dai, J. Deng, G. Bai, K. Ji and Y. Liu, *Environmental science & technology*, 2012, **46**, 4034-4041.

Journal of Materials Chemistry A Accepted Manuscript

29. F. Shi, F. Wang, H. Dai, J. Dai, J. Deng, Y. Liu, G. Bai, K. Ji and C. T. Au, *Applied Catalysis A: General*, 2012, **433-434**, 206-213.
30. S. C. Kim and W. G. Shim, *Applied Catalysis B: Environmental*, 2010, **98**, 180-185.
31. V. P. Santos, M. F. R. Pereira, J. J. M. Órfão and J. L. Figueiredo, *Applied Catalysis B: Environmental*, 2010, **99**, 353-363.
32. F. N. Aguero, B. P. Barbero, L. Gambaro and L. E. Cadús, *Applied Catalysis B: Environmental*, 2009, **91**, 108-112.
33. J. Hou, Y. Li, L. Liu, L. Ren and X. Zhao, *Journal of Materials Chemistry A*, 2013, **1**, 6736.
34. A. R. Gandhe, J. S. Rebello, J. L. Figueiredo and J. B. Fernandes, *Applied Catalysis B: Environmental*, 2007, **72**, 129-135.
35. C. Zhang, C. Wang, W. Zhan, Y. Guo, Y. Guo, G. Lu, A. Baylet and A. Giroir-Fendler, *Applied Catalysis B: Environmental*, 2013, **129**, 509-516.
36. S. S. T. Bastos, J. J. M. Órfão, M. M. A. Freitas, M. F. R. Pereira and J. L. Figueiredo, *Applied Catalysis B: Environmental*, 2009, **93**, 30-37.
37. X. Li, L. Wang, Q. Xia, Z. Liu and Z. Li, *Catalysis Communications*, 2011, **14**, 15-19.
38. G. S. Pozan, *Journal of hazardous materials*, 2012, **221–222**, 124-130.
39. F. Jiao and P. G. Bruce, *Advanced Materials*, 2007, **19**, 657-660.
40. F. Jiao, A. Harrison, A. H. Hill and P. G. Bruce, *Advanced Materials*, 2007, **19**, 4063-4066.
41. T.-K. Tseng, H. Chu and H.-H. Hsu, *Environmental science & technology*, 2002, **37**, 171-176.
42. Z. Chen, Q. Yang, H. Li, X. Li, L. Wang and S. Chi Tsang, *Journal of Catalysis*, 2010, **276**, 56-65.
43. D. Zhang, L. Zhang, L. Shi, C. Fang, H. Li, R. Gao, L. Huang and J. Zhang, *Nanoscale*, 2013, **5**, 1127-1136.
44. Z. Shu, Y. Chen, W. Huang, X. Cui, L. Zhang, H. Chen, G. Zhang, X. Fan, Y. Wang, G. Tao, D. He and J. Shi, *Applied Catalysis B: Environmental*, 2013, **140-141**, 42-50.
45. M. I. Zaki, A. K. H. Nohman, C. Kappenstein and T. M. Wahdan, *Journal of Materials Chemistry*, 1995, **5**, 1081-1088.
46. L. Yu, G. Diao, F. Ye, M. Sun, J. Zhou, Y. Li and Y. Liu, *Catalysis Letters*, 2011, **141**, 111-119.
47. K. Jirátová, J. Mikulová, J. Klempa, T. Grygar, Z. Bastl and F. Kovanda, *Applied Catalysis A: General*, 2009, **361**, 106-116.
48. K. Frey, V. Iablokov, G. Sáfrán, J. Osán, I. Sajó, R. Szukiewicz, S. Chenakin and N. Kruse, *Journal of Catalysis*, 2012, **287**, 30-36.
49. S. C. Kim and W. G. Shim, *Journal of hazardous materials*, 2008, **154**, 310-316.
50. T. F. Garetto and C. R. Apesteguía, *Applied Catalysis B: Environmental*, 2001, **32**, 83-94.
51. H. Pan, M. Xu, Z. Li, S. Huang and C. He, *Chemosphere*, 2009, **76**, 721-726.
52. J. Deng, L. Zhang, H. Dai, Y. Xia, H. Jiang, H. Zhang and H. He, *The Journal of Physical Chemistry C*, 2010, **114**, 2694-2700.
53. J. Deng, L. Zhang, H. Dai, H. He and C. T. Au, *Industrial & Engineering Chemistry Research*, 2008, **47**, 8175-8183.
54. J. Xu, Y.-Q. Deng, Y. Luo, W. Mao, X.-J. Yang and Y.-F. Han, *Journal of Catalysis*, 2013, **300**, 225-234.

Journal of Materials Chemistry A Accepted Manuscript

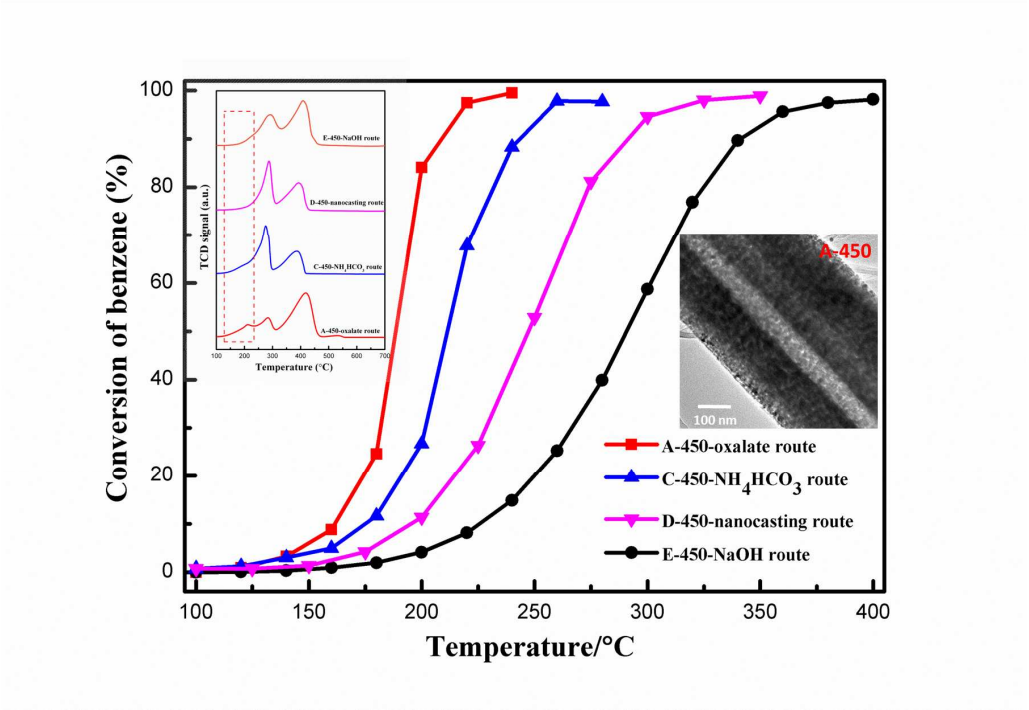

Highlight: Oxalate route was applied to synthesis mesoporous manganese oxides and its catalytic activity for VOCs oxidation was significantly promoted.

Journal of Materials Chemistry A Accepted Manuscript